UNIVERSITÄT AUGSBURG
Universitätsbibliothek

OPEN ACCESS
OPUS AUGSBURG

(II,Mn)VI nanostructures in mesoporous silica hosts –from powder samples to thin films

L. Chen, P. J. Klar, W. Heimbrodt, T. Kurz, Hans-Albrecht Krug von Nidda, Alois Loidl, A. V. Kouzema, M. Fröba

Angaben zur Veröffentlichung / Publication details:

Chen, L., P. J. Klar, W. Heimbrodt, T. Kurz, Hans-Albrecht Krug von Nidda, Alois Loidl, A. V. Kouzema, and M. Fröba. 2006. "(II,Mn)VI nanostructures in mesoporous silica hosts –from powder samples to thin films." *physica status solidi (b)* 243 (4): 831–34. https://doi.org/10.1002/pssb.200564609.

Nutzungsbedingungen / Terms of use:

licgercopyright

Dieses Dokument wird unter folgenden Bedingungen zur Verfügung gestellt: / This document is made available under these conditions:
Deutsches Urheberrecht
Weitere Informationen finden Sie unter: / For more information see:
https://www.uni-augsburg.de/de/organisation/bibliothek/publizieren-zitieren-archivieren/publiz/

(II,Mn)VI nanostructures in mesoporous silica hosts – from powder samples to thin films

L. Chen[1], **P. J. Klar**[*, 1], **W. Heimbrodt**[1], **T. Kurz**[2], **H.-A. Krug von Nidda**[2], **A. Loidl**[2], **A. V. Kouzema**[3], and **M. Fröba**[**, 3]

[1] Dept. Physics & Material Sciences Center, Philipps-University, Renthof 5, 35032 Marburg, Germany
[2] Institute of Physics & EKM, University of Augsburg, Universitätsstraße 1, 86159 Augsburg, Germany
[3] Institute of Inorganic and Analytical Chemistry, Justus-Liebig University, Heinrich-Buff-Ring 58, 35392 Gießen, Germany

1 Introduction

The synthesis of ordered arrays of dilute magnetic (II,Mn)VI semiconductor nanostructures inside the channels of mesoporous silica hosts in powder form is well established (for a review, see [1]). Such hybrids are of considerable interest from a fundamental point of view as the pore size of the hosts is adjustable in the range of 2 to 30 nm where quantum size effects are anticipated. This tunable pore size yields adjustable sharp upper limits of the guest particle size, allowing one to study the effect of the reduced dimensions on electronic and magnetic properties of the dilute magnetic semiconductors down to the smallest scales of interest. Recently the synthesis procedure was expanded from mesoporous powders to MTFs [2, 3] which should increase the technological relevance of these hybrid systems. Here, we demonstrate, first, that the $Cd_{1-x}Mn_xS$ nanostructures within MTF SiO_2 hosts (4 nm pores) and within MCM-41 mesoporous SiO_2 powders (3 nm pores) are comparable and, second, that the properties of the $Cd_{1-x}Mn_xS$ nanostructures are indeed strongly affected by the reduced lateral dimensions.

[*] Corresponding author: e-mail: peter.klar@physik.uni-marburg.de, Phone: +49 6421 282 1354, Fax: +49 6421 282 7036
[**] e-mail: michael.froeba@anorg.chemie.uni-giessen.de, Phone: +49 641 9934100, Fax: +49 641 9934109

2 Samples and experimental setup

The chemical synthesis of the two types of $Cd_{1-x}Mn_xS$ mesoporous silica hybrids comprises two steps, i.e. the synthesis of the mesoporous host and the intra-pore synthesis of the (II,Mn)VI semiconductor. The synthesis procedures as well as the structural characterization are described in detail for hybrids based on MCM-41 mesoporous SiO_2 hosts in powder form and for those based on SiO_2 MTF structures in Refs. [1] and [3], respectively. The Raman and the photoluminescence (PL) spectroscopic measurements were performed using standard set-ups. The EPR spectroscopy was conducted using X-band frequencies. Again, a detailed description of the set-ups can be found in Ref. [1].

3 Results and discussion

Figure 1 gives exemplarily results of the characterization of a $Cd_{0.9}Mn_{0.1}S$–MTF SiO_2 hybrid. Figure 1(a) is a transmission electron microscopic image (TEM) of a fraction of the hybrid. It clearly reveals the ordered pore structure of the host material which is still intact after intra-pore synthesis of the $Cd_{1-x}Mn_xS$ nanoparticles. The pores are about 4 nm in diameter. Figure 1(b) and (c) give proof that $Cd_{1-x}Mn_xS$ nanoparticles have formed inside the pores. The PL spectrum of the hybrid is dominated by the emission of the $Cd_{0.99}Mn_{0.01}S$ nanoparticles at about 2.1 eV. It is the so-called yellow emission band, which corresponds to the internal transition from the first excited state $^4T_1$ to the ground state $^6A_1$ within the $3d^5$ shell of Mn incorporated on cation site of a wide-gap II–VI semiconductor [4]. The corresponding PLE spectrum shows a distinct band gap feature which is considerably blue-shifted with respect to that of bulk $Cd_{0.99}Mn_{0.01}S$ (see also Fig. 2), as expected for nanoparticles with diameters smaller than 4 nm.

Figure 2 depicts a comparison of low-temperature band-gap energies obtained of bulk $Cd_{1-x}Mn_xS$ and $Cd_{1-x}Mn_xS$ nanostructures incorporated into SiO_2 MTFs and MCM-41 SiO_2 powders, respectively. The gap energies of both $Cd_{1-x}Mn_xS$ nanostructures show the same trends as a function of Mn content x and are, for all x, strongly blue-shifted with respect to bulk. The band gap dependence of both, bulk $Cd_{1-x}Mn_xS$ and the nanostructures, exhibits the so-called p–d exchange induced bowing with x [5]. The bowing seems to be slightly stronger in the nanostructures. This is very likely caused by a combination of electronic confinement and of altered magnetic properties due to the size reduction, as explained in Ref. [1].

Figure 3(a) shows the EPR spectra of a $Cd_{0.99}Mn_{0.01}S$–MTF SiO_2 hybrid (top) and that of a pristine SiO_2 MTF host. The analysis of the two spectra reveals that the feature with the hyperfine structure at about 330 mT is related to the $Cd_{1-x}Mn_xS$ nanostructures whereas the features at 75 mT and 155 mT are due to Fe^{3+} impurities in the glass substrate [6] used for the preparation of the MTF. The additional broad feature in the pristine MTF which is also at about 330 mT is due to the resonator background. The EPR

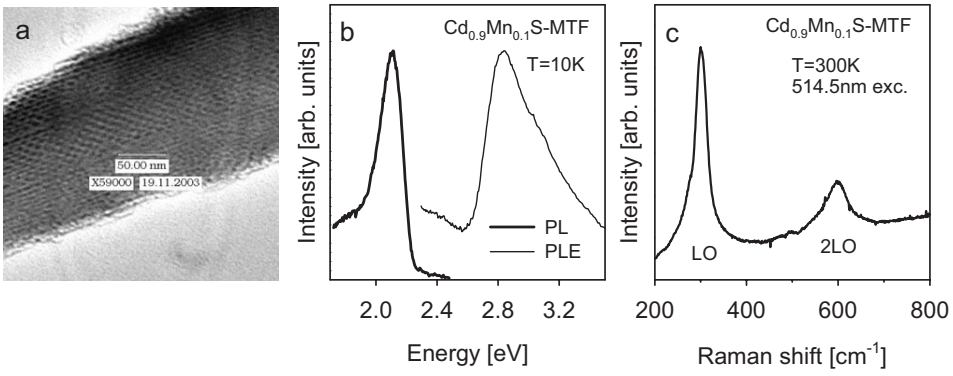

Fig. 1 Characterization of a $Cd_{0.9}Mn_{0.1}S$–MTF SiO_2 hybrid: (a) TEM; (b) PL and PLE; (c) Raman spectroscopy.

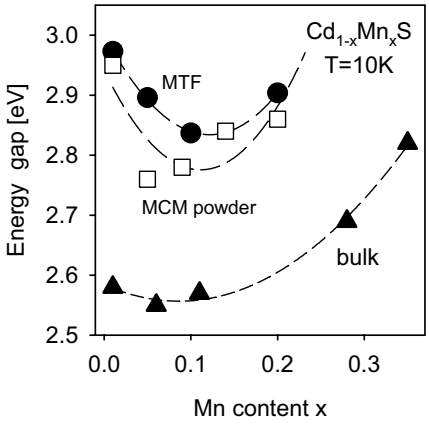

Fig. 2 Band-gap energies at 10 K of bulk $Cd_{1-x}Mn_xS$ and $Cd_{1-x}Mn_xS$ nanostructures incorporated into SiO_2 MTFs and MCM-41 SiO_2 powders, respectively.

spectra of the $Cd_{1-x}Mn_xS$-MTF SiO_2 hybrids corrected for substrate and resonator effects, are shown in Fig. 3(b) as a function of x. A typical EPR spectrum of exchange-coupled Mn^{2+} ions in (II,Mn)VI alloys [7] consists of a sextet of sharp lines with a splitting of about 7 mT between neighboring lines, each line with a pair of satellites at lower magnetic field on a broad Lorentzian background. The spectrum is centered around a g-factor of 2. The sharp lines and their satellites correspond to the allowed and forbidden hyperfine transitions of the six Zeeman-split $m_S = -5/2, \ldots, +5/2$ levels of the $^6S_{5/2}$ (or $^6A_1$) ground state of the Mn^{2+} 3d-electrons. The spectra of the nanostructures exhibit an additional sextet structure with a hyperfine splitting of about 9.5 mT corresponding to Mn aggregated at the surface the $Cd_{1-x}Mn_xS$ nanoparticles [8] which persists with increasing x whereas the signal contribution from the bulk of the nanostructure becomes purely Lorentzian at higher x. EPR spectra of all samples were measured in the range between 4 and 300 K. After correction for substrate and resonator effects, the EPR spectra were analyzed in terms of EPR intensity and line width of the Lorentzian main signal.

The EPR intensity in the paramagnetic phase is proportional to the magnetic susceptibility $\chi \propto (T + \theta)^{-1}$ where θ is the Curie–Weiss parameter. The Curie–Weiss parameter extracted in the high

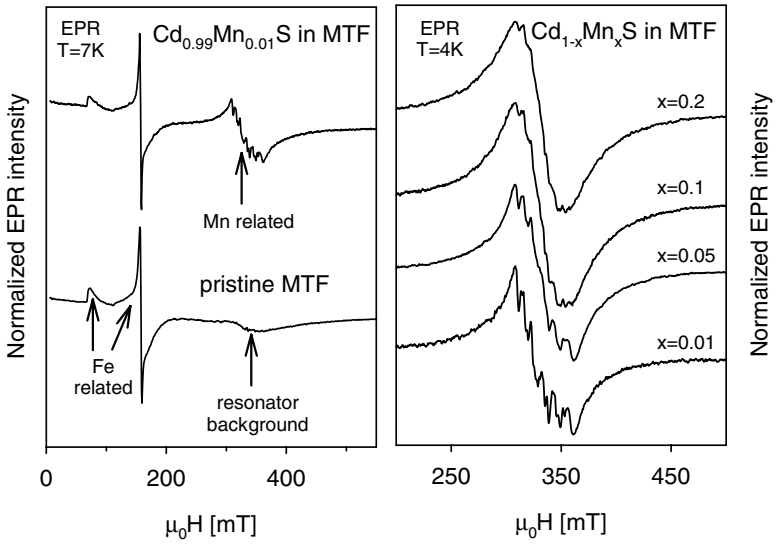

Fig. 3 (a) Normalized EPR spectra of a $Cd_{0.99}Mn_{0.01}S$–MTF SiO_2 hybrid and a pristine SiO_2 MTF. (b) EPR spectra of $Cd_{1-x}Mn_xS$ nanostructures of various x synthesized in SiO_2 MTFs after subtraction of the EPR spectrum of pristine SiO_2 MTF.

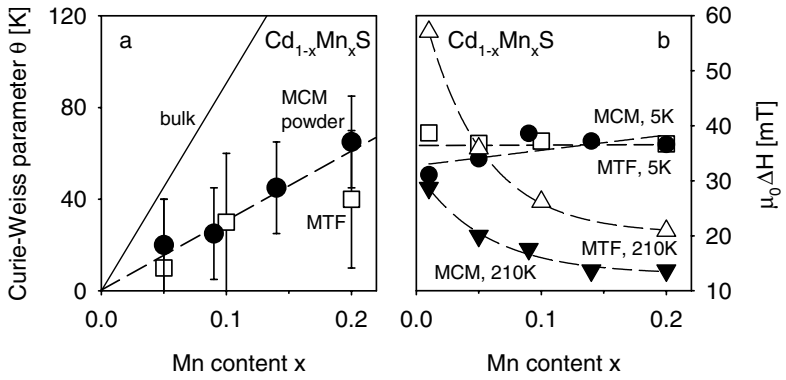

Fig. 4 Comparison of the EPR results of $Cd_{1-x}Mn_xS$ nanostructures synthesized in MTF and MCM powder, respectively. (a) Curie–Weiss parameter; (b) EPR line width at 5 K and 210 K, respectively.

temperature limit is indicative for the effective antiferromagnetic nearest neighbor and next-nearest neighbor coupling between the Mn ions within the II–VI host. For bulk in the high temperature limit, it holds in mean field approximation that $\theta = 2/(3k_B) \cdot S(S+1) \cdot x \cdot [J_{nn}z_{nn} + J_{nnn}z_{nnn}]$ where J_{nn} (J_{nnn}) is the coupling constant between (next) nearest-neighbor Mn spins and z_{nn} (z_{nnn}) is the number of (next) nearest-neighbor sites, and $S = 5/2$ is the Mn spin. In nanostructures θ is considerably smaller due to an effective reduction of z_{nn} and z_{nnn} close to the surface [1]. This is also seen in Fig. 4(a) where the Curie–Weiss parameters of both types of nanostructures are comparable and show an almost linear dependence on x (dashed line), which is significantly lower than the corresponding dependence for bulk $Cd_{1-x}Mn_xS$ (solid line).

Figure 4(b) depicts a comparison of the concentration dependence of the EPR line width of $Cd_{1-x}Mn_xS$ nanostructures synthesized within MCM-41 SiO_2 powder (solid symbols) and within SiO_2 MTF (open symbols), respectively. Again the behaviour is almost the same. At low temperatures (5 K), where the nearest-neighbor Mn ions have formed antiferromagnetically coupled pairs which do not contribute to the magnetism in the magnetic field range of the EPR, the linewidth is almost constant as a function of x for the two types of nanostructures and basically given by the width of the hyperfine structure. At higher temperatures (210 K) where the antiferromagnetically coupled pairs are broken up an exchange narrowing effect can be observed, i.e. the line width decreases with increasing x.

4 Conclusions

Our measurements show that the electronic and the magnetic properties, and thus the quality, of $Cd_{1-x}Mn_xS$ nanoparticles incorporated into thin mesoporous SiO_2 films is comparable to those inside mesoporous MCM-41 SiO_2 powders. This presents an important step towards the technological use of these nanostructures.

Acknowledgement We are grateful for funding by the DFG and the BMBF.

References

[1] F. J. Brieler, P. Grundmann, M. Fröba, L. Chen, P. J. Klar, W. Heimbrodt, H.-A. Krug von Nidda, T. Kurz, and A. Loidl, Eur. J. Inorg. Chem. 3597–3611 (2005).
[2] C. Tura, N. Coombs, and Ö. Dag, Chem. Mater. **17**, 573 (2005).
[3] A. V. Kouzema, M. Fröba, L. Chen, P. J. Klar, and W. Heimbrodt, Adv. Funct. Mater. **15**, 168 (2005).
[4] O. Goede and W. Heimbrodt, phys. stat. sol. (b) **146**, 11 (1988).
[5] R. B. Bylsma, W. M. Becker, J. Kossut, and U. Debska, Phys. Rev. B **33**, 8207 (1986).
[6] T. Castner Jr., G. S. Newell, W. C. Holton, and C. P. Slichter, J. Chem. Phys. **32**, 668 (1960).
[7] Y. J. Ishikawa, J. Phys. Soc. Jpn. **21**, 1473 (1966).
[8] P. H. Borse, D. Srinivas, R. F. Shinde, S. K. Date, W. Vogel, and S. K. Kulkarni, Phys. Rev. B **60**, 8659 (1999).